Frequency-tunable high-Q superconducting resonators via wireless control of nonlinear kinetic inductance

Cite as: Appl. Phys. Lett. **114**, 192601 (2019); https://doi.org/10.1063/1.5098466 Submitted: 02 April 2019 . Accepted: 22 April 2019 . Published Online: 13 May 2019

Mingrui Xu, Xu Han, Wei Fu, Chang-Ling Zou 🗓, and Hong X. Tang







ARTICLES YOU MAY BE INTERESTED IN

High-T_C superconducting detector for highly-sensitive microwave magnetometry Applied Physics Letters 114, 192602 (2019); https://doi.org/10.1063/1.5090175

Frequency-tunable superconducting resonators via nonlinear kinetic inductance Applied Physics Letters 107, 062601 (2015); https://doi.org/10.1063/1.4927444

Néel vector reorientation in ferromagnetic/antiferromagnetic complex oxide nanostructures Applied Physics Letters 114, 192403 (2019); https://doi.org/10.1063/1.5094604





Frequency-tunable high-Q superconducting resonators via wireless control of nonlinear kinetic inductance

Cite as: Appl. Phys. Lett. **114**, 192601 (2019); doi: 10.1063/1.5098466 Submitted: 2 April 2019 · Accepted: 22 April 2019 · Published Online: 13 May 2019 · Corrected 1 August 2019







Mingrui Xu, 1,a) Xu Han, 1,a) Wei Fu, Chang-Ling Zou, 2 1 and Hong X. Tang 1,b)

AFFILIATIONS

Department of Electrical Engineering, Yale University, New Haven, Connecticut 06520, USA

ABSTRACT

Frequency-tunable microwave resonators are in great demand especially in hybrid systems where precise frequency alignment of resonances is required. Here, we present frequency-tunable high-Q superconducting resonators fabricated from thin niobium nitride and niobium titanium nitride films. The resonant frequency is tuned by applying a magnetic field perpendicular to the hole structures in the resonator's inductor wire, whose kinetic inductance is modified by wirelessly induced DC supercurrents. A continuous *in situ* frequency tuning of over 300 MHz is achieved for a 10 GHz resonator with a moderate magnetic field of 1.2 mT. The planar resonator design and the noncontact tuning scheme greatly ease the fabrication complexity and can be widely applied in many hybrid systems for coupling microwave modes with other forms of excitations such as optical photons, phonons, magnons, and spins.

Published under license by AIP Publishing. https://doi.org/10.1063/1.5098466

As an essential building block of future quantum technology, superconducting microwave resonators have been extensively studied for interfacing with other forms of excitations, including phonons, nagnons, spins, optical photons, and superconducting qubits. Such hybrid systems leverage the strength of superconducting circuits and other quantum systems and thus are considered as a promising approach toward the realization of scalable quantum networks. To achieve desired coupling between the microwave mode and other excitations, fine frequency alignment is routinely required. Hence, frequency tunability of microwave resonators can be of great value. In addition, frequency-tunable microwave resonators have versatile applications in superconducting circuits, such as tunable microwave filters, microwave parametric amplifiers, 10–12 magnetometers, and microwave storage.

Common approaches to realizing frequency-tunable microwave resonators include the use of Josephson junctions ^{15–18} and high-kinetic-inductance superconducting wires. ^{19–21} The high nonlinearity of Josephson junctions permits the large frequency tuning range. However, the junctions have limited critical current (typically less than several microamps) and require a relatively complex fabrication process. On the other hand, high-kinetic-inductance wires can be easily

patterned because of their simple geometries and hence are a more accessible source of nonlinearity. In addition, they are suitable for applications that require larger operating power²² or exposure to larger magnetic fields, ²¹ because superconducting materials of high-kinetic-inductance wires usually have higher critical temperatures (T_c) than most accessible Josephson junctions. Exploiting the current dependence of kinetic inductance, ²³ frequency-tunable microwave resonators have been demonstrated by adding an extra circuit to the resonator for injecting a DC current into the microwires. ^{20,24} The magnetic field dependence of kinetic inductance has also been utilized to enable frequency-tunable microwave resonators. ^{19,21} Typically, to obtain a wide tuning range, a large magnetic field (\sim 100 mT) is needed. ²¹

In this article, we present a junction-free, high-Q superconducting microwave resonator with a frequency tuning range of 3.5% from 10 GHz. In the presence of a moderate magnetic field on the order of milliTesla, supercurrents are induced around the hole structures in the resonator due to the magnetic shielding effect of superconductors. These screening currents modify the kinetic inductance and hence shift the resonant frequency. Since the screening currents are generated wirelessly in the resonator

 $^{^2}$ Key Laboratory of Quantum Information, University of Science and Technology of China, CAS, Hefei, Anhui 230026, China

a)Contributions: M. Xu and X. Han contributed equally to this work.

b) Electronic mail: hong.tang@yale.edu

without additional DC wire connections, the resonator can maintain a high quality factor (*Q* factor). This wireless frequency tuning scheme can be applied in different hybrid systems for precise *in situ* frequency tuning and alignment.

Shown in Fig. 1(a) is the frequency-tunable microwave resonator named "Ouroboros," because of its resemblance to a snake biting its own tail. Ouroboros has been previously exploited for achieving multimode strong coupling with bulk acoustic modes. The devices are fabricated from two types of superconductors: a niobium titanium nitride (NbTiN) film sputtered on a silicon substrate and a niobium nitride (NbN) film deposited on a sapphire substrate via atomic layer deposition. Both films have thicknesses of 50 nanometers. The device patterns are defined by one single e-beam lithography step using a hydrogen silsesquioxane (HSQ) resist, followed by chlorine dry etching. The remaining HSQ mask is removed using diluted buffered oxide etch. The structure of the Ouroboros can be understood as a planar LC resonator—an arc-shaped microwire as the inductor and a disk as the capacitor [see Fig. 1(b)]. Hence, the resonant frequency is inversely proportional to the square root of the inductance, which is composed of geometric inductance $L_{\rm m}$ and kinetic inductance $L_{\rm k}$, $f_{\rm c} = \frac{1}{\sqrt{(L_{\rm m} + L_{\rm k})C}}$

While the geometric inductance $L_{\rm m}$ is fixed after the device is fabricated, the kinetic inductance $L_{\rm k}$, originating from the kinetic energy of electrons, can be tuned by current.^{23,25} To wirelessly induce DC currents in the inductor wire of the Ouroboros, hole structures are patterned in the inductor wire [see Fig. 1(a) zoomed-in view]. When an

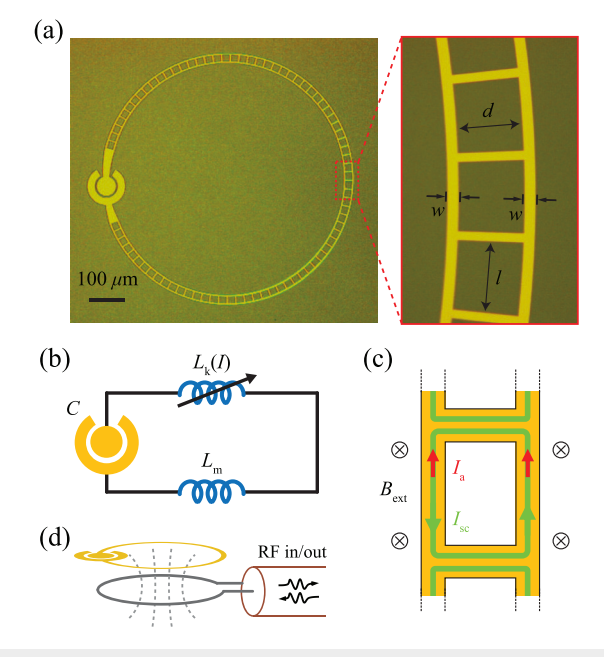


FIG. 1. (a) Optical micrograph of a tunable Ouroboros resonator with design parameters labeled in the zoomed-in view on the right. (b) Equivalent circuit of the tunable Ouroboros resonator, whose inductance is constituted of both geometric inductance $L_{\rm m}$ and kinetic inductance $L_{\rm k}(I)$. (c) Frequency tuning mechanism by kinetic inductance. $I_{\rm sc}$: DC screening currents induced by the external magnetic field. $I_{\rm a}$: AC current of the resonant mode. (d) Readout scheme of the Ouroboros via inductive coupling to a loop antenna made from a coaxial cable.

external magnetic field $B_{\rm ext}$ is applied perpendicular to the device plane, screening DC supercurrents

$$I_{\rm sc} \approx B_{\rm ext} \frac{d}{\mathcal{L}_{\rm sc}}$$
 (1)

will be induced circulating around the holes to expel magnetic flux from penetration [illustrated in Fig. 1(c)]. Here, d denotes the width of each hole, and $\mathcal{L}_{\rm sc}$ is the effective geometric inductance per unit length for the circulating DC current $I_{\rm sc}$. For small $I_{\rm sc}$ ($I_{\rm sc}/I^* \ll 1$), the kinetic inductance increases with it quadratically 26

$$L_{\rm k}(I_{\rm sc}) \approx L_{\rm k0} \left[1 + \left(\frac{I_{\rm sc}}{I^*} \right)^2 \right],$$
 (2)

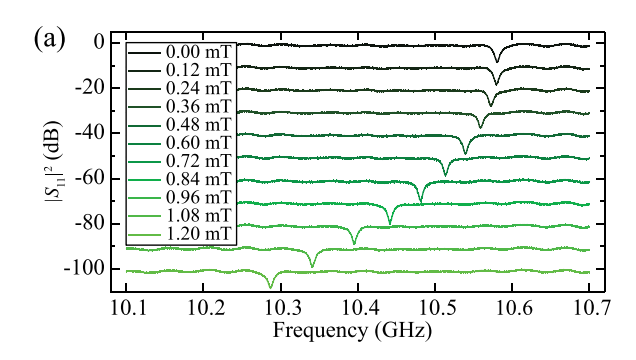
where L_{k0} is the kinetic inductance at zero current, and I^* is a characteristic current on the order of the critical current. When the change of inductance is small enough $\left(\frac{\Delta L_k}{L_k + L_m} \ll 1\right)$, the resonant frequency f_c linearly shifts with it, $\frac{\Delta f_c}{f_c} \approx -\frac{1}{2} \frac{\Delta L_k}{L_k + L_m}$. Considering Eqs. (1) and (2), we get

$$\frac{\Delta f_c}{f_c} \approx -kB_{\rm ext}^2,$$
 (3)

where $k=\frac{1}{2}\frac{L_{\rm ko}}{L_{\rm ko}+L_{\rm m}}\frac{1}{I^{*2}}\frac{d^2}{\mathcal{L}_{\rm sc}^2}$. As a result, the Ouroboros resonant frequency can be quadratically tuned by the external magnetic field. It is notable that the wireless-tuning scheme is not unique to the Ouroboros structure. It can be easily adapted in other forms of superconducting resonators.

To characterize the resonance and the frequency tunability, each Ouroboros is inductively coupled to a loop antenna made from a coaxial cable, for sending in and reading out RF signals [Fig. 2(d)]. A superconducting coil is placed above the Ouroboros to provide a perpendicular magnetic field. The whole setup is then enclosed in a copper box and soaked in liquid helium (T = 4.2 K) for a low temperature measurement. Reflection spectra (S11) of an Ouroboros at different external magnetic fields are shown in Fig. 2(a). Each Lorenztian shaped dip marks the Ouroboros resonant frequency at a magnetic field. When the magnetic field increases from 0 to 1.2 mT, a continuous frequency tuning of 350 MHz from a 10.6 GHz resonance is achieved. The relative frequency tuning and the intrinsic Q_{in} of a set of different devices are shown in Fig. 2(b). A large relative tuning range above 3% is obtained for both devices made from NbN and NbTiN films. Each frequency tuning curve shows a good quadratic dependence on the magnetic field B_{ext} , as suggested by Eq. (3). The intrinsic Qin measured at 4.2 K is on the order of a few thousands without significant deterioration in the presence of the magnetic field.

By comparing the tunability of five otherwise identical devices with different hole widths [see curves #1–#5 in Fig. 2(b)], it is evident that a larger hole width leads to more efficient frequency tuning. Compared to the device with hole width $d=10~\mu m$, it takes 5 times less magnetic field for the device with $d=50~\mu m$ to obtain the same resonant frequency shift of 3%. This trend is important because when operating in a cryostat, a low magnetic field is always preferred to minimize its influence on other superconducting components as well as the heat generation from the coil current. To quantitatively study the different tuning efficiency of each device, each tuning curve is fit to



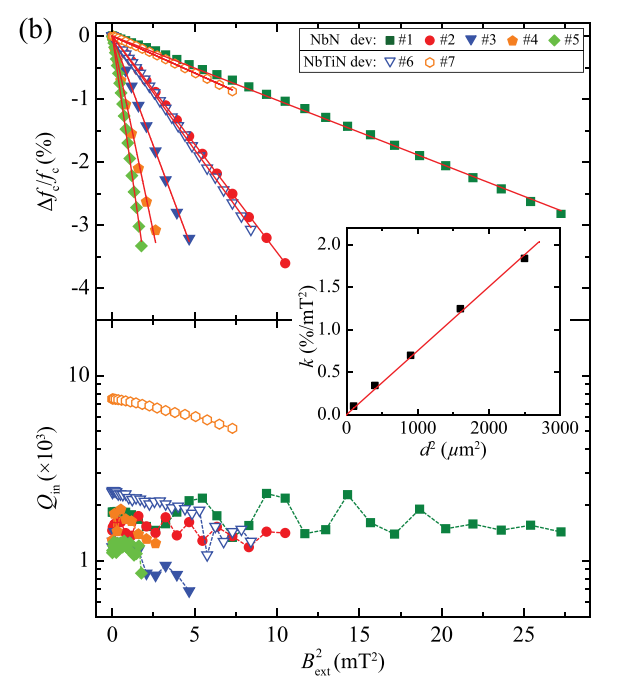


FIG. 2. Frequency tuning of tunable Ouroboros devices at 4.2 K. (a) The evolution of $|S_{11}|^2$ spectra when the magnetic field is swept from 0 to 1.2 mT. The *y*-axis values are offset for illustration purposes. (b) Relative resonant frequency shift and intrinsic Q as a function of $B_{\rm ext}^2$. Devices #1–#5 are made from NbN with the same wire width $w=1~\mu{\rm m}$ but different hole widths d=10, 20, 30, 40, and 50 $\mu{\rm m}$, respectively. Devices #6 and #7 are made from NbTiN with the same hole width $d=30~\mu{\rm m}$ but different wire widths w=1 and 5 $\mu{\rm m}$. All the devices have center resonant frequencies at around 10 GHz. The inset shows quadratic coefficients k extracted from tuning curves #1–#5 as a function of d^2 . The green diamond curves (#5) correspond to the device in (a).

Eq. (3) to find the quadratic coefficient k, shown as solid lines in Fig. 2(b). k values extracted from fittings for the 5 NbN devices are plotted in the inset of Fig. 2(b), which is proportional to d^2 . This observation is consistent with our theory, because under the same external magnetic field, the amount of induced DC screening supercurrents is proportional to the width of the holes, see Eq. (1). In principle, \mathcal{L}_{sc} also increases with d. However, since the gap between two parallel wires on both sides of the holes d is much greater than the wire width w, the change of \mathcal{L}_{sc} is negligible.

Making narrower wires also optimizes the device's tunability. Curves #6 and #7 in Fig. 2(b) are characteristics of two similar devices

with $1-\mu$ m-wide and $5-\mu$ m-wide wires, respectively. Comparison between these two curves shows that the device with a reduced wire width has superior tunability. One reason narrower wires are favorable to this application is because they have a higher kinetic inductance participation ratio $\frac{L_{k0}}{L_{k0}+L_m}$. As the kinetic inductance of a microwire is inversely proportional to its cross-section area, and the geometric inductance is relatively insensitive to the change of the width, narrower wire results in a larger kinetic inductance participation ratio. The kinetic inductance of the superconducting microwires can be estimated by measuring the sheet resistance $R_{\rm sq}$ at room temperature and the critical temperature T_c of the film.²³ For the NbTiN film, characterization results are $R_{\rm sq}=34~\Omega/\Box$ and $T_{\rm c}=13.0~{\rm K}$; hence, the sheet kinetic inductance is estimated to be $L_{k0,sq} \approx 4 \ pH/\Box$. Estimated from a flat inductor wire model,²⁷ the geometric inductance of a 50-nmthick, 1-µm-wide wire is 1.6 nH/mm, which reduces to 1.3 nH/mm for a 5-μm-wide wire. Thus, for a 50-nm-thick NbTiN wire, by reducing the wire width from 5 μ m to 1 μ m, the kinetic inductance participation ratio is boosted from 38% to 71%.

Once the magnetic field is increased beyond a certain value, the resonant frequency will abruptly jump back [after the cut-offs of curves in Fig. 2(b)] and the resonant frequency exhibits hysteresis behavior upon reverse sweeping of the magnetic field. This phenomenon sets the limit of the frequency tuning range. It can be attributed to the fluxon penetration²⁸ through the hole structures as the screening current density in the inductor wire exceeds a certain threshold.

Finally, we characterize the device performance at a lower temperature. A frequency-tunable Ouroboros [device #5 in Fig. 2(b)] is mounted on the still flange of a dilution refrigerator, and then, the frequency tuning curve and the Q factors are measured at 800 mK. As shown in Fig. 3, the device's intrinsic $Q_{\rm in}$ has significantly improved to 10^5 compared with a few thousand at 4.2 K. More importantly, within the tuning range of 2% at 1 mT, the high intrinsic $Q_{\rm in}$ is maintained with only a mild deterioration of less than 20%. In principle, this frequency tuning scheme does not introduce any additional loss to the device when the magnetic field is not applied, 19 so it is suitable for applications where very high Q is required.

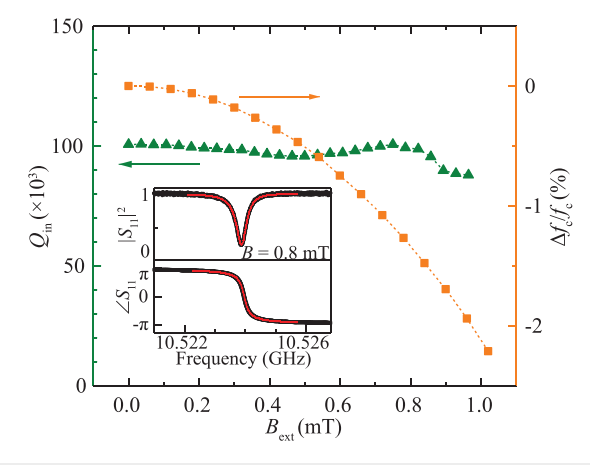


FIG. 3. Intrinsic $Q_{\rm in}$ and relative frequency shift of Ouroboros at 800 mK. The inset shows a reflection spectrum with a Lorentzian fitting at a magnetic field of 0.8 mT. A weak RF probe tone of $-80\,{\rm dBm}$ is used to make sure the device is in the linear regime

In conclusion, we demonstrated that by patterning simple hole structures in the high-kinetic-inductance wire of a superconducting resonator, a large frequency tuning range of a few percent with a high Q of 10⁵ can be obtained. Compared to other frequency tuning schemes based on kinetic inductance, our approach eliminates additional circuits for injecting DC currents^{20,24} and is also more efficient than direct magnetic field tuning—the required magnetic field for 3% resonant frequency shift has been reduced by two orders of magnitudes from the best result reported.²¹ To further boost the frequency tunability, narrower and thinner wires as well as wider holes can be exploited. The demonstrated technique can be readily incorporated in other superconducting hybrid systems for fine frequency alignment. Moreover, the kinetic inductance nonlinearity in our design can be further exploited for parametric amplification. Depending on whether a DC magnetic bias is applied, both four-wave mixing and three-wave mixing can be realized under proper microwave pump tones.

The authors thank M. H. Devoret for his original idea of adding patterned holes in the microresonators and critical reading of this manuscript. The authors thank L. Jiang for inspirational discussions, and M. Power, J. Agresta, C. Tillinghast and M. Rooks for assistance in device fabrication. This project is funded by LPS/ARO under Grant Nos. W911NF-14-1-0563 and W911NF-18-1-0020. H.X.T. acknowledges partial support from AFOSR MURI Grant (FA9550-15-1-0029), NSF EFRI Grant (EFMA-1640959), DOE Grant (DE-SC0019406), and the Packard Foundation.

REFERENCES

- ¹J. Teufel, T. Donner, D. Li, J. Harlow, M. Allman, K. Cicak, A. Sirois, J. D. Whittaker, K. Lehnert, and R. W. Simmonds, Nature 475, 359 (2011).
- ²X. Han, C.-L. Zou, and H. X. Tang, Phys. Rev. Lett. 117, 123603 (2016).
- ³A. Tkalčec, S. Probst, D. Rieger, H. Rotzinger, S. Wünsch, N. Kukharchyk, A. D. Wieck, M. Siegel, A. V. Ustinov, and P. Bushev, Phys. Rev. B **90**, 075112 (2014).
- ⁴H. Huebl, C. W. Zollitsch, J. Lotze, F. Hocke, M. Greifenstein, A. Marx, R. Gross, and S. T. B. Goennenwein, Phys. Rev. Lett. 111, 127003 (2013).
- ⁵D. I. Schuster, A. P. Sears, E. Ginossar, L. DiCarlo, L. Frunzio, J. J. L. Morton, H. Wu, G. A. D. Briggs, B. B. Buckley, D. D. Awschalom, and R. J. Schoelkopf, Phys. Rev. Lett. **105**, 140501 (2010).

- ⁶A. Bienfait, J. J. Pla, Y. Kubo, M. Stern, X. Zhou, C. C. Lo, C. D. Weis, T. Schenkel, M. L. W. Thewalt, D. Vion, D. Esteve, B. Julsgaard, K. Mølmer, J. J. L. Morton, and P. Bertet, Nat. Nanotechnol. 11, 253 (2015).
- ⁷L. Fan, C.-L. Zou, R. Cheng, X. Guo, X. Han, Z. Gong, S. Wang, and H. X. Tang, Sci. Adv. 4, eaar4994 (2018).
- ⁸A. Blais, R.-S. Huang, A. Wallraff, S. M. Girvin, and R. J. Schoelkopf, Phys. Rev. A **69**, 062320 (2004).
- ⁹M. H. Devoret and R. J. Schoelkopf, Science **339**, 1169 (2013).
- ¹⁰S. Chaudhuri, D. Li, K. Irwin, C. Bockstiegel, J. Hubmayr, J. Ullom, M. Vissers, and J. Gao, Appl. Phys. Lett. 110, 152601 (2017).
- ¹¹E. A. Tholén, A. Ergül, E. M. Doherty, F. M. Weber, F. Grégis, and D. B. Haviland, Appl. Phys. Lett. **90**, 253509 (2007).
- ¹²M. A. Castellanos-Beltran and K. W. Lehnert, Appl. Phys. Lett. 91, 083509 (2007)
- ¹³J. Luomahaara, V. Vesterinen, L. Grönberg, and J. Hassel, Nat. Commun. 5, 4872 (2014).
- ¹⁴M. Pierre, I.-M. Svensson, S. R. Sathyamoorthy, G. Johansson, and P. Delsing, Appl. Phys. Lett. **104**, 232604 (2014).
- ¹⁵N. Bergeal, F. Schackert, M. Metcalfe, R. Vijay, V. E. Manucharyan, L. Frunzio, D. E. Prober, R. J. Schoelkopf, S. M. Girvin, and M. H. Devoret, Nature 465, 64 (2010).
- ¹⁶M. Sandberg, C. M. Wilson, F. Persson, T. Bauch, G. Johansson, V. Shumeiko, T. Duty, and P. Delsing, Appl. Phys. Lett. **92**, 203501 (2008).
- ¹⁷Z. L. Wang, Y. P. Zhong, L. J. He, H. Wang, J. M. Martinis, A. N. Cleland, and Q. W. Xie, Appl. Phys. Lett. **102**, 163503 (2013).
- ¹⁸B. Abdo, A. Kamal, and M. Devoret, Phys. Rev. B **87**, 014508 (2013).
- ¹⁹J. E. Healey, T. Lindström, M. S. Colclough, C. M. Muirhead, and A. Y. Tzalenchuk, Appl. Phys. Lett. 93, 043513 (2008).
- ²⁰M. R. Vissers, J. Hubmayr, M. Sandberg, S. Chaudhuri, C. Bockstiegel, and J. Gao, Appl. Phys. Lett. 107, 062601 (2015).
- ²¹N. Samkharadze, A. Bruno, P. Scarlino, G. Zheng, D. P. DiVincenzo, L. DiCarlo, and L. M. K. Vandersypen, Phys. Rev. Appl. 5, 044004 (2016).
- ²²B. H. Eom, P. K. Day, H. G. LeDuc, and J. Zmuidzinas, Nat. Phys. 8, 623 (2012).
- ²³A. J. Annunziata, D. F. Santavicca, L. Frunzio, G. Catelani, M. J. Rooks, A. Frydman, and D. E. Prober, Nanotechnology 21, 445202 (2010).
- ²⁴A. A. Adamyan, S. E. Kubatkin, and A. V. Danilov, Appl. Phys. Lett. 108, 172601 (2016).
- ²⁵M. Tinkham, *Introduction to Superconductivity* (Courier Corporation, 2004).
- ²⁶J. Zmuidzinas, Annu. Rev. Condens. Matter Phys. 3, 169 (2012).
- ²⁷B. C. Wadell, *Transmission Line Design Handbook* (Artech House, 1991).
- ²⁸D. Bothner, T. Gaber, M. Kemmler, D. Koelle, R. Kleiner, S. Wünsch, and M. Siegel, Phys. Rev. B 86, 014517 (2012).